Free Gait Transition and Stable Motion Generation Using CPG-based Locomotion Control for Hexapod Robots

Chen Ji
Huzhou Institute of Zhejiang University
Fan Li
fanli77@zju.edu.cn
Huzhou Institute of Zhejiang University
Xu Chao
Huzhou Institute of Zhejiang University

Research Article

Keywords: Central pattern generator (CPG), Gait generation, Gait transition, Hexapod robot

Posted Date: August 9th, 2024

DOI: https://doi.org/10.21203/rs.3.rs-4734634/v1

Additional Declarations: No competing interests reported.

Free Gait Transition and Stable Motion Generation Using CPG-based Locomotion Control for Hexapod Robots

Ji Chen[1*], Li Fan[1*] and Chao Xu[1]

[1*]Huzhou Institute, Zhejiang University, Street, Huzhou, 313000, Zhejiang, China.

*Corresponding author(s). E-mail(s): ji.chenuk@gmail.com; fanli77@zju.edu.cn;
Contributing authors: cxu@zju.edu.cn;

Abstract

In this paper, we address the problem of gait transition for legged robots, focusing on the challenges of versatile phase transitions and stable motion generation. To tackle the phase transition problem, we begin by analyzing the undesirable phase-lock phenomenon and identifying the phase lock conditions for conventional diffusively coupled nonlinear oscillators. We then propose a novel diffusive Central Pattern Generator (CPG) model and theoretically prove its ability to handle phase transitions across various gait patterns. For the stability problem during transitions from one gait to another, we introduce a motion generation framework that provides an interface for stability criteria, enabling smooth trajectory adjustments based on the robot's stability. We evaluate the proposed method using both simulations and a physical hexapod robot. Experimental results demonstrate that our approach can achieve transitions across a wide range of gait patterns while ensuring stable and smooth motion during the transitions.

Keywords: Central pattern generator (CPG), Gait generation, Gait transition, Hexapod robot

1 Introduction

"Gait" refers to the distinct pattern or sequence of limb movements used by legged creatures during locomotion. Multi-legged animals have multiple gait patterns available and tend to choose specific gait patterns for specific requirements. Researches

show that gait patterns are chosen based on speed requirements. For example, the metachronal gait in hexapodal locomotion is associated with low-speed movements, while the tripod gait is linked to high-speed maneuvers [1][2]. Moreover, contemporary research reveals that environmental stimuli also play an important role in choosing the gait patterns. For instance, terrestrial arthropods widely use the high-speed metachronal gait during rapid escape maneuvers [3]. And, honeybees utilize tetrapod gaits when navigating smooth surfaces or terrains [4]. Aside from versatile gait patterns that the animals have, they can also unconsciously manage smooth and stable transition from one gait to another. Over the last two decades, fully transferring the maneuverability of the multi-legged animals to the multi-legged robots remains an open topic.

Neurobiological findings indicate that central pattern generators (CPGs) located in the spinal cord governs the generation of animal gaits [5][6]. Compared to the various models that mimic the mechanism of the biological CPGs, the models of coupled nonlinear dynamical systems have solid theoretical background, i.e. in group and bifurcation theory [7]. The locomotion framework based on nonlinear coupled systems are widely used in many bio-inspired robots such as snake-like robot [8], quadruped robot [9][10] and hexapod robot [11][12]. In recent years, research on these models have increasingly focused on fluent gait transitions. Theorists have propose enhanced nonlinear dynamic systems capable of facilitating these transitions. For example, Wei Xiao et al. (2014) propose a structure with synaptic-coupled Hopf Oscillators [13], while Yu et al. introduce a diffusive-coupled Van der Pol Oscillators [14]. Both models achieve gait transitions by adjusting the coupling schemes, namely the phase lags between cells. Both models' ability to transition from low-speed to high-speed gaits has been confirmed. A particularly promising structure is embodied by the delayed Van der Pol oscillators [8], where researchers examine the system's bifurcation and show that different parameter regions correspond to various spatio-temporal patterns. However, unlike the phase lag or coupling strength integral to other CPG formulations, the precise physical connotation of the gait parameter remains unclear. We have implemented the aforementioned coupled nonlinear oscillators and found that certain design limitations in some dynamic systems result in a significantly narrower range of achievable gait transitions for artificial CPGs compared to their biological counterparts. For example, the phase-lock phenomenon, an undesirable occurrence during the gait transition process, restricts diffusive-CPGs [14] to a limited range of gait transitions (between tripod, tetrapod, and wave gaits). Completely solving this undesirable phase-lock phenomenon will fully liberate the phase transition ability of this type of artificial CPG model.

Another persistent issue in the gait transition process is ensuring the robot's safety during all types of transitions. Current approaches to address this issue are primarily twofold: trajectory adjustment and gait pattern selection. For trajectory adjustment, Yu et al. (2016)[14] consider the stance trajectory with a consistent stance speed to ensure smooth motion during the transition. This method is effective in preventing disruptions during the transition but is incomplete as it does not consider stability criteria. Regarding gait pattern selection methods, Darbha (2017)[15] constructs and analyzes a loss function that considers stability during the gait transition. The author

suggests that the transition should occur at an optimal time point to maximize the loss function and enhance stability, though this approach shows limitations in flexibility. Both Bai et al. (2019)[16] and Shaw et al. (2022)[17] consider the selection of valid gait patterns during the transition. However, gait pattern selection is a discontinuous method, and smoothly connecting these distinct patterns remains a tricky problem.

To fully comprehend the intricate logic of animal gait transitions, we face two main challenges: developing an artificial CPG model that supports a more diverse gait transitions and constructing a motion control strategy that ensures stable movements throughout these transitions. Our study explores the undesirable phase-lock phenomena that often obstruct gait transitions across different types of CPGs. Building on our analysis and the work of Yu et al. (2016), we propose an enhanced CPG model that permits a broader range of gait transitions while maintaining superior limit cycle behavior. Additionally, we introduce a new trajectory planning scheme that provides a straightforward interface for stability criteria, allowing reasonable trajectory adjustments based on the robot's stability.

The structure of this paper is as follows: Section II dissects the commonplace phase-lock phenomena at the gait transition stage in coupled cell systems; Section III presents our enhanced CPG model that enables a wider range of gait transitions; Section IV describes our motion generation method and corresponding leg control strategy for hexapod robots with consideration of the stability criteria; Section V provides validation for the effectiveness of our proposed model; and finally, Section VI concludes our paper.

2 Undesirable phase-lock phenomena of diffusive-CPG model

2.1 Diffusive-CPG model

In this chapter, we analyze the undesirable phase-locking (we use UPL later for simplicity) behavior of conventional diffusive-CPG model [14]. Within this framework, the dynamics of the neuron's state vector $z_i \in \mathbb{R}^2$ are governed by the following set of differential equations:

$$\dot{z}_i = \begin{cases} F(z_i) + \gamma(R(\theta_i)z_{i+1} - z_i), & \text{for } i = 1, 2, ...N-1, \\ F(z_i) + \gamma(R(\theta_i)z_1 - z_i), & \text{for } i = N. \end{cases} \tag{1}$$

Here, $F(z_i)$ represents the internal dynamics of the neuron, and γ is a constant parameter. Typically, the internal dynamics of neurons are described using Hopf or Van der Pol oscillators. The term $R(\theta_i)$ is a clockwise rotation matrix, with θ_i indicating the desired phase lag between the i-th and $i+1$-th neuron. N is always set to be an even number, indicating the number of the cells. The term "diffusive" indicates that the states of the i-th neuron are only affected by the states of the $i+1$-th neuron. The topology of the diffusive-CPG network with N neurons is depicted in Fig. 1a.

To explain how the dynamics governing phase shifts between neurons, we define the term $\gamma(R(\theta_i)z_{i+1} - z_i)$ as δ_i. This term can be interpreted as an augmented velocity

that directs the state of the i-th neuron towards that of the $(i+1)$-th neuron, as illustrated in Fig. 1b. When $\delta_1 = \delta_2 = \ldots = \delta_N = 0$, the states of all neurons are synchronized, exhibiting a phase lag of $\varphi_{i+1} - \varphi_i = \theta_i$ for all i. The term δ_i can be further decomposed into components perpendicular and parallel to z_i, denoted as ${}^{\perp}\delta_i$ and ${}^{\parallel}\delta_i$, respectively. The primary factor influencing the phase shift of the neuron states is ${}^{\perp}\delta_i$. Consequently, the influence of ${}^{\parallel}\delta_i$ will be disregarded in the subsequent analysis of UPL.

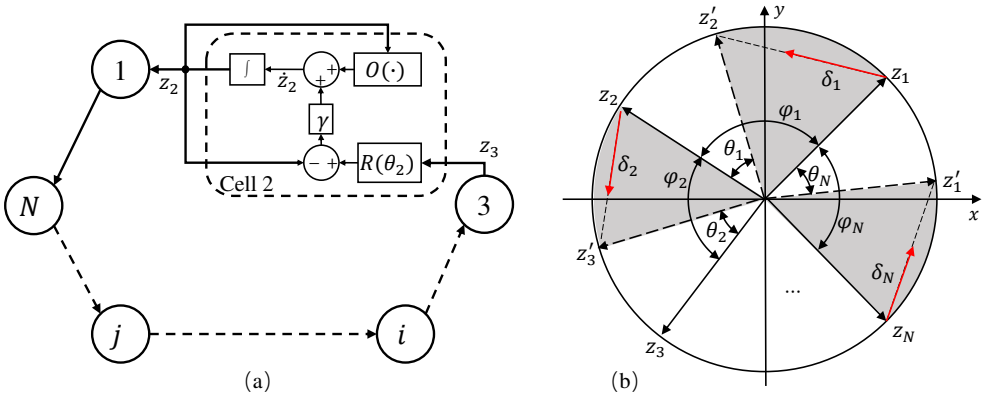

Fig. 1: Structure of the original diffusive-CPG network (a). An illustration that portrays the phase transient process of diffusive-CPG model (b), where $z'_{i+1} = R(\theta_i)z_{i+1}$ and $\delta_i = \gamma(z'_i - z_i)$.

2.2 UPL analysis of diffusive-CPG model

By adjusting each neuron's desired phase-lag θ_i, we can achieve the phase transition between different gaits. As reported in the study by Yu et al. [14], the synchronization error of the system described by Eq. (1) is uniformly ultimately bounded (UUB), implying that the phase relations will converge to the desired phase lags as $t \to \infty$. However, the UUB analysis is primarily qualitative. In the present work, we identify UPL phenomenon, which significantly slows down the transient process but does not contradict the theorem presented in the previous paper [14]. The UPL phenomenon occurs during the transient process. To analyze it, we delve directly into the differential equations. Our basic assumption is that the execution of the gait transition is only allowed at the steady state (stable limit cycle) of the dynamical system.

To analyze the UPL phenomenon, we propose a loose definition of it for coupled cell systems.

Definition 1. *For coupled cell systems, an undesirable phase-lock emerges during the phase transition towards the desired phase lags θ_i. Such a phase-lock is said to exist if there are at least two cells, i and $i+1$, which satisfy the following condition:*

$$\varphi_{i+1}(t) - \varphi_i(t) = \theta_{PL} \neq \theta_i, \qquad \textit{for } t_{PL} < t < t_{\max} \tag{2}$$

where φ_i and φ_{i+1} represent the actual phases of the state vectors for cell i and $i+1$ respectively. Meanwhile, θ_i denotes the desired phase-lag between cell i and $i+1$. t_{PL} designates the time point when $\varphi_{i+1}(t) - \varphi_i(t)$ converges to the UPL angle θ_{PL}. In the inequality $t_{\max} >> t_{PL}$, $t_{\max}$ indicates that the phase-lags between cell i and $i+1$ maintain the lock at the angle θ_{PL} for a substantial duration.

It's noteworthy that UPL generally arises from design issues in coupling terms. In CPG models, despite the impedance created by the coupling terms, the actual phase lag may converge to intended phase-lags within a finite timeframe due to the nonlinearity of the internal oscillator $F(z)$. However, this convergence is highly slow und uncontrollable, rendering it unsuitable for gait transitions, which need to be completed swiftly. Hence, this situation is also deemed as an undesirable phase-lock scenario. With regards to a regular diffusive-CPG model, we present a proposition to demonstrate that UPL happens globally in all neurons in diffusive-CPG model.

Proposition 1. *Consider a model of diffusively coupled nonlinear oscillators, with system dynamics governed by Equation (1). Given a neuron i and its successive neuron $i+1$, if they are identified to be in an UPL situation denoted by $\langle i, i+1 \rangle$, then it follows that the states across all neurons are also in an UPL situation, expressed as:*

$$\langle 1, 2, \ldots, i-1, i, i+1, \ldots, N \rangle. \tag{3}$$

Furthermore, in this scenario, all the state vectors exhibit a constant angular velocity, denoted as ω_{PL}.

Proof. Assume that for times $t > t_{PL}$, two neurons indexed by i and $i+1$ are phase-locked with a phase-lag θ_{PL}. This assumption establishes the following relation:

$$z_i(t) = R(\theta_{PL}) z_{i+1}(t), \quad \text{for } t > t_{PL} \tag{4}$$

To maintain a specific phase-lag θ_i, it is required that the augmented velocities δ_i and δ_{i+1} induce identical angular velocities between z_i and z_{i+1}. With the circular orbit assumption, this requirement can be expressed by:

$$\delta_i = R(\theta_{PL}) \delta_{i+1}, \quad \text{for } t > t_{PL} \tag{5}$$

Expanding and simplifying this relationship yields:

$$R(\theta_i) z_{i+1}(t) - z_i(t) = R(\theta_{PL})(R(\theta_{i+1}) z_{i+2}(t) - z_{i+1}(t)), \tag{6}$$

$$R(\theta_i) z_{i+1}(t) = R(\theta_{PL}) R(\theta_{i+1}) z_{i+2}(t), \quad \text{for } t > t_{PL}. \tag{7}$$

Equation (7) implies that if neuron pairs i and $i+1$ are phase-locked after a coupling modification, their successive neurons $i+1$ and $i+2$ will also maintain a constant phase relationship for $t > t_{PL}$. The desired phase relationship between these subsequent neurons is θ_{i+1} . Conversely, according to Eq. (7), the actual phase

relationship between neurons $i+1$ and $i+2$ is computed as

$$\theta_{PL_{i+1}} = \theta_{PL} - \theta_i + \theta_{i+1}. \tag{8}$$

Then, with the relation $\theta_{PL} \neq \theta_i$, the following inequality holds:

$$\theta_{PL_{i+1}} \neq \theta_{i+1}. \tag{9}$$

This indicates that the succeeding neuron pair $i+1$ and $i+2$ also exhibit the UPL phenomenon. Consequently, the sequence $\langle i, j\rangle$ can be extended to $\langle i, i+1, i+2\rangle$. Since these three neurons are phase-locked, they rotate at the same angular speed ω_{PL} .

Iterating the process from Eq. (4) to Eq. (9), the phase-lock list can be extended to all neurons, denoted as:

$$\langle 1, 2, \ldots, i, i+1, i+2, \ldots, N\rangle. \tag{10}$$

□

From Proposition 1, we can deduce several interesting corollaries. For the first corollary, we consider the scenario where the phase lags remain unchanged after switching to the desired phase lag.

Corollary 1. *For a model of diffusively coupled nonlinear oscillators, with system dynamics governed by Equation (1), let the desired phase-lag before and after the transition be θ^A and θ^B respectively. The phase relation between the cells remains unchanged after changing the desired phase-lag from θ^A to θ^B if and only if for any cells i and $i+1$,*

$$\theta^B_{i+1} - \theta^A_{i+1} = 2\pi n(\theta^B_i - \theta^A_i), \tag{11}$$

where n is an integer.

Proof. At time $t > t_A$, when transferring from gait A to gait B, if the phases are undesirably locked at θ^A, according to Proposition 1, the state vectors z_{i+1} and z_{i+2} obey the constant phase relation:

$$z_{i+1}(t) = R(\theta^A_{i+1}) z_{i+2}(t) \text{ for } t > t_A. \tag{12}$$

Then, for Eq. (7) with $\theta_{PL} = \theta^A_i$, we can rewrite the equation in this situation as

$$R(\theta^B_i) z_{i+1}(t) = R(\theta^A_i) R(\theta^B_{i+1}) z_{i+2}(t), \quad \text{for } t > t_{PL}. \tag{13}$$

We left-multiply both sides of the equation by $R^{-1}(\theta^B_i)$ to obtain the following formula:

$$z_{i+1}(t) = R^{-1}(\theta^B_i) R(\theta^A_i) R(\theta^B_{i+1}) z_{i+2}(t), \quad \text{for } t > t_{PL}. \tag{14}$$

Using Eq. (12), the formulation can be further simplified into

$$z_{i+1}(t) = R^{-1}(\theta^B_i) R(\theta^A_i) R(\theta^B_{i+1}) R^{-1}(\theta^A_{i+1}) z_{i+1}(t), \quad \text{for } t > t_{PL}. \tag{15}$$

Consequently, we have the following relationship:

$$R(\theta_i^B)R^{-1}(\theta_i^A)z_{i+1}(t) = R(\theta_{i+1}^B)R^{-1}(\theta_{i+1}^A)z_{i+1}(t), \quad \text{for } t > t_{PL}. \tag{16}$$

Obviously, Eq. (16) requires the same rotation angles, as described in Eq. (11), on both sides to achieve equivalence.

Furthermore, the "only if" statement can be derived by calculating the angular speeds when Eq. (11) is met. Under this condition, the angular velocity difference between the state vectors of the cells remains zero after switching from θ^A to θ^B. Apart from the augmented angular velocities acting on z_i, there are no other sources that can alter the phase relations between the cells. Consequently, the relative phases among the cells remain unchanged, and the undesired phase-lock phenomenon occurs. □

From the result of Corollary 1, we can also conclude the corollary of reverse phase transition:

Corollary 2. *For a model of diffusively coupled nonlinear oscillators, with system dynamics governed by Equation (1), if the phase transition from gait A to gait B cannot be achieved (i.e., the gait patterns remain at A after $t > t_{PL}$), then the reverse phase transition from gait B to gait A cannot be achieved either.*

Proof. According to Corollary 1, if the phase transition from A to B was failed, then the coupling scheme, i.e. the desired phase lags of gait A and B satisfy the precondition of phase-lock, as described in Eq. (11). We take the negative sign at both side of the equation. And we can see that for the phase-transition from B to A,

$$\theta_{i+1}^A - \theta_{i+1}^B = 2\pi n(\theta_i^A - \theta_i^B) \quad \forall i, j. \tag{17}$$

Based on corollary 1, the phase transition from B to A cannot be achieved. □

The theoretical results presented in Corollary 1 and Corollary 2 provide a streamlined framework for verifying the transferability of gaits within a standard diffusive CPG model. To illustrate this, let us consider the specific scenario of generating hexapodal gaits. Regrettably, the phase transitions encompassing tripod, metachronal, and caterpillar gaits cannot be achieved by a six-cell diffusive-CPG in any direction. We will explicate this fundamental limitation extensively in the forthcoming experimental section.

The question now is whether the phase lags will lock at an intermediate angle between the start phase lag θ_i^A and the target phase-lag θ_i^B? We suppose it will not happen and propose our hypothesis.

Hypothesis 1. *For the phase transition process of the dynamical system governed by the differential equations (1), where the current phase lags are denoted as θ_i^A and the desired phase lags are denoted as θ_i^B , if the system is not phase-locked at the current phase lags θ_i^A , then it will not become phase-locked at any other intermediate phase lags. Instead, the system will ultimately converge to the desired phase lags θ_i^B in a relatively short amount of time.*

Our hypothesis is grounded in the dynamical properties of the unstable equilibrium points within the system's phase space. Specifically, we posit that the system's states will depart from these unstable equilibrium points even in the presence of minor disturbances. Furthermore, since the UPL phenomenon was not observed at the initial states, as per the UUB analysis reported in [14], we expect the system's states to converge to the desired phase lags θ_i^B at a relatively quick speed. This rapid convergence implies that the system's states will quickly pass through any intermediate UPL states, which have been identified as unstable equilibrium points. In other words, the definition of UPL is effectively confined to the transient locking at the current phase lags θ_i^A during the system's transient process. And, as a result, our ultimate goal is clearer: create a model that will not phase-lock at the start phase lags during the transient process.

3 Improved Diffusive-CPG model

In this section, we propose an improved diffusive-CPG model that achieves free phase transition and exhibits enhanced phase-transition dynamics. As mentioned in the section 2.1, the parameter γ influences both the amplitude of the velocity augmentation tangential and co-linear to z_i. When γ is sufficiently large, the co-linear component can dramatically alter the shape of the limit cycle during the transition process, which not only complicates the phase-shift analysis but also adversely impacts the control of limbs' motion. To address this issue, we adopt map Perp : $\mathbb{R}^2 \to \mathbb{R}^2$, with $\text{Perp}_{z_i}(v_i) =^{\perp} v_i$. Here, $v_i = R(\theta_i)z_{i+1} - z_i$ is defined as the velocity augmentation and ${}^{\perp}v_i$ represents the component of v_i that is perpendicular to z_i.

The internal structure of the CPG cell model is illustrated in Fig. 2.

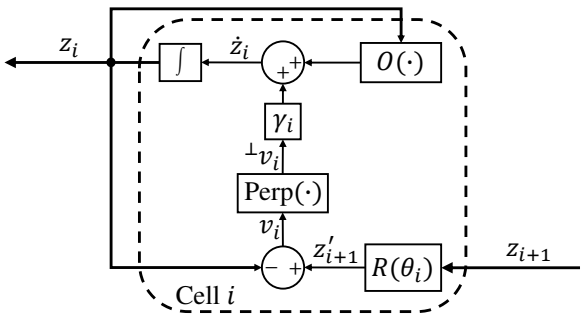

Fig. 2: Illustration of the cell structure of the proposed diffusive-CPG model. Here, the state vector z_{i+1} are transmitted to the i-th neuron to impact i-th state vector. Ideally, the Perp function only chooses the velocity augmentation that perpendicular to z_i, which will not impact the shape of the limit cycle.

In this model, as the term ${}^{\perp}v_i$ is perpendicular to z_i, the velocity augmentations only affect the states' phase shift, regardless of the magnitude of the parameter γ_i. This maintains the shape of the limit cycle during the transient process to be **circular**. This

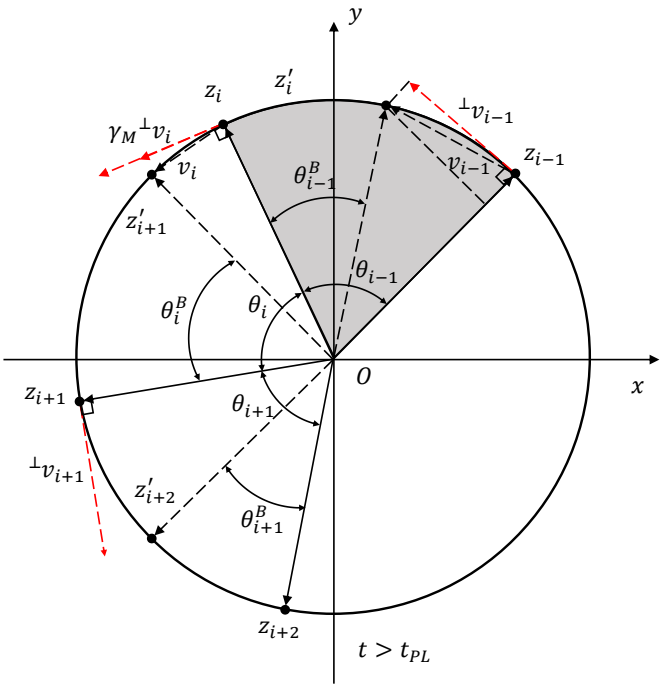

Fig. 3: Illustration of the transient process of a variation of diffusive-CPG model.

optimizes the transition dynamics and simplifies the analysis. The system dynamics of the model are described using the following differential equations:

$$\dot{z}_i = \begin{cases} F(z_i) + \gamma_i \mathrm{Perp}_{z_i}(R(\theta_i) z_{i+1} - z_i), & \text{for } i = 1, 2, \ldots N-1, \\ F(z_i) + \gamma_i \mathrm{Perp}_{z_i}(R(\theta_i) z_1 - z_i), & \text{for } i = N. \end{cases} \tag{18}$$

Fig. 3 show an illustration that portrays the phase relations and augmented velocities during the phase-transition process

For the proposed CPG model, when $\gamma_i = \gamma_j$ for all i and j, according to Proposition 1, the phase-locked state is propagated to all the cells. We consider the scenario when $\gamma_i \neq \gamma_j$ for all i and j, and propose the Proposition 2.

Proposition 2 (Avoiding Phase-Locking during Transition)**.** *Consider a diffusively coupled network of nonlinear oscillators, where the system dynamics are governed by Equation* (18)*. Suppose the desired phase-lag before and after the phase transition is* θ^A *and* θ^B*, respectively.*

Then, there exists a set of parameters $\{\gamma_i\}$ *such that the system can avoid potential phase-locking at* θ_i^A *during the phase transition process.*

Proof. According to the problem setup, during the phase transition process, all state vectors z_i exhibit a limit cycle with a fixed radius r. As shown in Fig. 3, at time t, the

phase-shift between z_i and z_{i+1} is $\varphi_i(t)$. We can calculate the chord length l_i between z_i and z'_{i+1} using the following geometric relationship:

$$l_i = 2r \sin \frac{\varphi_i(t) - \theta_i^B}{2} \tag{19}$$

The augmented angular velocity of the state vector z_i is then given by:

$$\Delta\omega_i = \gamma_i l_i \cos(\frac{\varphi_i(t) - \theta_i^B}{2})/r = 2\gamma_i \sin \frac{\varphi_i(t) - \theta_i^B}{2} \cos(\frac{\varphi_i(t) - \theta_i^B}{2}) = \gamma_i \sin(\varphi_i(t) - \theta_i^B) \tag{20}$$

As shown in Eq. (20), the augmented angular velocities depend solely on the difference between the current phase relation φ_i and the desired phase relation θ_i^B, as well as the coupling strength γ_i.

Assume that the UPL happens after the start of the phase transition, and the phases are locked at θ_i^A. Then, the augmented angular velocity for each cell i can be calculated as:

$$\Delta\omega_i = \gamma_i sin(\theta_i^A - \theta_i^B) \tag{21}$$

For the UPL to occur, according to Proposition 1, all state vectors must rotate at the same angular speed, i.e., $\Delta\omega_1 = \Delta\omega_2 = \cdots = \Delta\omega_N$.

For gait specifications, the desired phase-lag between the cells are $\theta_i^B = \frac{2\pi k_i^B}{N}$ and $\theta_i^A = \frac{2\pi k_i^A}{N}$, where $k_i^A, k_i^B \in \mathbb{N}$. We can derive the following relationship:

$$\gamma_i \sin(\theta_i^A - \theta_i^B) = \gamma_j \sin(\theta_j^A - \theta_j^B) \tag{22}$$

$$\gamma_i \sin(\frac{2\pi}{N}(k_i^A - k_i^B)) = \gamma_j \sin(\frac{2\pi}{N}(k_j^A - k_j^B)) \tag{23}$$

$$\frac{\gamma_i}{\gamma_j} = \frac{\sin(\frac{2\pi}{N}(\Delta k_j))}{\sin(\frac{2\pi}{N}(\Delta k_i))}, \tag{24}$$

where $\Delta k_i = k_i^A - k_i^B$. Since $k_i \in \mathbb{N}$, then $\Delta k_i \in \mathbb{Z}$. For a fixed N, the values of $\sin(\frac{2\pi}{N}(\Delta k_i))$ lie in a set with a limited number of elements.

We can then find a set of $\{\gamma_i\}$ such that the ratio $\frac{\gamma_i}{\gamma_j}$ does not match the ratio of the sine functions. This contradicts the previous assumption of UPL at θ_i^A. Therefore, with a proper choice of the γ parameters, the undesired phase-locking (UPL) at θ_i^A will not occur. □

Moreover, according to the Hypothesis 1, the UPL would not happen globally.

To construct the computation model of the proposed CPG model, we provide a process to perform the mapping Perp_{z_i}. The process is about to calculate ${}^{\perp}v_i$. Defining $z'_{i+1} = R(\theta_i)z_{i+1}$, and $v_i = z'_{i+1} - z_i$. Then the magnitude $\|{}^{\perp}v_i\|$ and direction $n_{{}^{\perp}v_i}$ are calculated as:

$$\|{}^{\perp}v_i\| = \|v_i\| \cos(\theta_l), \tag{25}$$

$$n_{\perp_{v_i}} = \frac{R(\theta_l)v_i}{\|v_i\| + \epsilon}. \tag{26}$$

In Eq. (25) and (26), θ_l represents the signed half-angle between z'_{i+1} and z_i, given by:

$$\theta_{l_i} = \frac{1}{2}\text{sign}(z'_{i+1} \times z_i) \arccos \frac{z'_{i+1} \cdot z_i}{\|z'_{i+1}\|\|z_i\| + \epsilon}. \tag{27}$$

For the equations evolving division calculations, we use a small positive real value ϵ to prevent the singularities.

In the proposed CPG model, due to the effect of the Perp_{z_i} term, the state vectors rotates around the cyclic limit cycle with the fixed radius r. We can then simply calculate the phase angle of each cell's state vector and normalize them to the phase signal $\tau_i \in [0, 1]$.

4 CPG-based locomotion control for hexapod robot

This section aims to develop a locomotion strategy for a hexapod robot based on the proposed CPG model. The overall locomotion generation process is illustrated in Fig. 4. This process takes manual inputs (turning ρ and gait specifications) and utilizes phase signals τ_1 through τ_6 from the CPG model to calculate each leg's desired joint angles.

The proposed foot-tip motion generator considers stability during gait transitions and enables turning. We introduce two criteria to enhance stability during the gait transition process: (1) The phase transition should only affect the swing speed of the legs in the swing stage, while the legs in the stance stage maintain a consistent speed. (2) The legs in the swing stage must automatically adjust their touchdown time, adhering to the stability criterion. Additionally, we interpret the robot's turning as the rotation of its center around a fundamental circular path with radius R_T , as depicted by the blue arc in Fig. 5. The turning parameter ρ is then defined as $\rho = 1/R_T$. Under this setting, when the turning radius R_T approaches infinity, the robot's motion aligns with its x-axis. Conversely, when R_T tends towards zero, the robot rotates around its z-axis. To ensure the geometric validity of the turning mechanism, the robot's foot-tips must be positioned on concentric circles of the fundamental circular path. An example of such a concentric circle for Leg 1 and Leg 4 is depicted as the green arc in Fig. 5. Considering these aspects, the detailed trajectory planning for the stance and swing stages is as follows.

4.1 Stance Trajectory Planning

Based on the stability criterion 1 and Fig. 5, each stance foot-tip maintains the same angular velocity $\dot{\psi}_L$ around their concentric turning circles, which is calculated as follows:

$$\dot{\psi}_L = \frac{\omega_0 lmax}{2\pi\beta}, \tag{28}$$

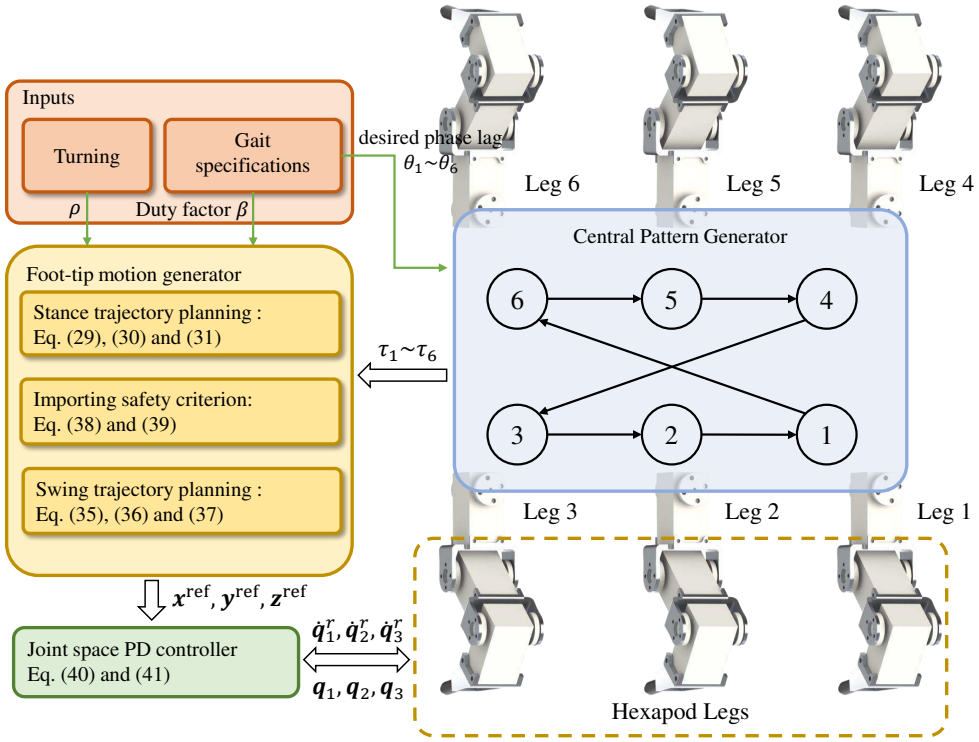

Fig. 4: An illustration of the CPG-based locomotion control framework.

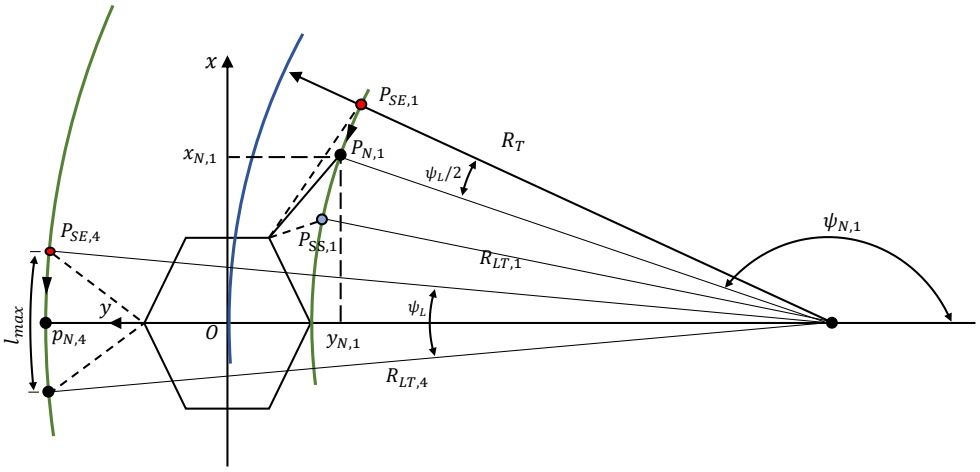

Fig. 5: An illustration of the foot-tip trajectory calculation. We consider leg 1 as an example, where $p_1^N = (x_1^N, y_1^N)$ represents the neutral position of Leg 1.

where l_{max} is a constant describing the step-size of the leg that is furthest from the center of rotation at stable gait patterns, ω_0 is the inherent angular frequency of the oscillator $F(z_i)$ in Eq. (18), and β is the duty cycle corresponding to the gait pattern, which is calculated as the ratio of the stance time and the total time of the walking cycle.

The reference stance trajectory for the i^{th} arbitrary leg in the base link's Cartesian space is calculated as:

$$x_{st,i}^{\text{ref}}(t) = R_{LT,i}\sin(\psi_i(t-1) + \dot{\psi}_L\Delta t), \tag{29}$$

$$y_{st,i}^{\text{ref}}(t) = R_T - R_{LT,i}\cos(\psi_i(t-1) + \dot{\psi}_L\Delta t), \tag{30}$$

$$z_{st,i}^{\text{ref}}(t) = H_0. \tag{31}$$

This trajectory describes the foot-tip rotating around its concentric circle with angular speed $\dot{\psi}_L$. In the formulas, $R_{LT,i}$ is the turning radius of the i-th leg, H_0 is a constant stance height parameter, and Δt is the loop duration of the control cycle. Given the reference foot-tip position at the previous step, $\mathbf{p}_i^{\text{ref}}(t-1) = (x_i^{\text{ref}}(t-1), y_i^{\text{ref}}(t-1))$, the term $\psi_i(t-1)$ is computed as:

$$\psi_i(t-1) = \pi - \arctan\left(\frac{x_i^{\text{ref}}(t-1)}{R_T - x_i^{\text{ref}}(t-1)}\right) \tag{32}$$

Furthermore, given each foot-tip's neutral position $\mathbf{p}_{N,i} = (x_{N,i}, y_{N,i})$, the radius of the concentric circle for the i^{th} leg is computed as:

$$R_{LT,i} = \sqrt{(x_{N,i})^2 + (R_T - y_{N,i})^2}. \tag{33}$$

4.2 Swing Trajectory Planning

While the stance trajectories consider the walking velocities to prevent interlimb contradictions, the swing trajectories must consider the phase transition and stability issues during the gait transitions. To address this, we first use De Casteljau's algorithm [18] to generate a Bézier curve for the swing stage. The Bézier-shaped swing trajectory, as shown in Fig. 6, is generated by three control points:

$$P_{SE,i} = (\psi_{N,i} - \frac{\psi_L}{2}, 0),\ P_{SS,i} = (\psi_{STE,i}, 0),\ P_{SH,i} = (\frac{P_{SE}[1] + P_{SS}[1]}{2}, H_1). \tag{34}$$

$P_{SE,i}$ is the fixed swing end point, which is depicted as red dots in Fig. 5. $P_{SS,i}$, depicted as a blue dot, is the swing start point, and we set its ψ coordinate value equal to the ψ value of Leg i at the end of its last stance phase, symbolized as $\psi_{STE,i}$. $P_{SH,i}$ is the control point that controls the height that the leg raises, with the parameter H_1.

The internal progression of the swing trajectories is governed by the Bézier parameter $p \in [0, 1]$. The point $(\psi_{sw,i}(p), z_{sw,i}(p))$ represents a specific location on the curve, where $\psi_{sw,i}(p)$ denotes the angle formed by the foot-tip, the rotation center, and the y-axis, and $z_{sw,i}(p)$ represents the elevation height of the foot-tip.

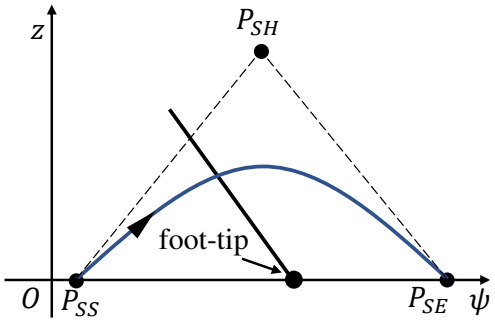

Fig. 6: An illustration of swing trajectory generated by Bézier curve. The swing trajectories locate in the ψOz coordinate, where ψ indicates the angle formed by foot-tip point, turning center and the y axis of the robot baselink frame.

Based on the Bézier trajectory, the reference foot-tip positions in Cartesian coordinates with respect to the baselink frame are calculated as follows:

$$x_{sw,i}^{ref}(t) = R_{LT,i}\sin(\psi_{sw,i}(p)), \tag{35}$$

$$y_{sw,i}^{ref}(t) = R_T - R_{LT,i}\cos(\psi_{sw,i}(p)), \tag{36}$$

$$z_{sw,i}^{ref}(t) = z_{sw,i}(p). \tag{37}$$

The relationship between the Bézier curve's internal progression and the phase signal from the CPG model is given by:

$$p = k\frac{\tau_i - \beta}{1-\beta}, \tag{38}$$

where β is the duty cycle. As p controls the evolution of the swing trajectory and is coupled with the phase signal from the CPG model, the swing trajectory can effectively follow the phase transitions dictated by the CPG model. Additionally, the swing stage plays a crucial role in enhancing stability during the gait transition process. When the stability criterion is satisfied, we set $k = 1$ to allow for a pure phase transition in the swing stage. Conversely, if the stability criterion is not met, we set $k > 1$ to accelerate the progression of p, thereby transitioning the swing legs to stance legs more quickly to provide additional supports.

The key point now lies in the choice of the stability criterion. Various criteria, such as the static stability margin calculated by the support polygon and the tip-over stability measure [19], can be used to control the evolution of the swing stage. We propose a computationally effective stability measure. We divide the legs located on the left and right sides of the robot into left and right side-groups. We then calculate the warning score for each side-group to control the swing progress of the legs in that

group. The group warning score is calculated as follows:

$$WS_g = \begin{cases} 1, & \tau_{l\in g} < \beta \text{ and } \tau_{m\in g} > \beta \text{ and } \tau_{n\in g} > \beta \\ 0. & \text{otherwise} \end{cases} \tag{39}$$

In this formula, g indicates the side group containing the legs l, m, and n. The warning score WS_g is set to one when only one leg is in the stance phase. Under this scenario, the swing progress of the legs in the same side-group should be accelerated by setting the k parameter greater than 1 in Eq. (38). This ensures a faster transition from the swing phase to the stance phase, enhancing stability by providing increased support.

4.3 Controllers

We use velocity-based controllers [20] to track the swing and the stance phase trajectory plan $p^{\text{ref}}(t)$:

$$u(t) = K_p(p^{\text{ref}}(t) - p(t)) + \dot{p}^{\text{ref}}(t), \tag{40}$$

where K_p is a proportional-derivative (PD) gain matrix, and $p(t)$ is the foot tip's position at time t. This controller allows the foot tip to closely follow the desired trajectory during the swing and stance phase. Given the control signal u in Cartesian space, we can then calculate the joint space command of each foot-tip as:

$$\dot{q}^r(t) = J^{\dagger}u(t), \tag{41}$$

where J is the Jacobain matrix that maps the joint velocities to the linear and angular velocities of the foot-tips in base-link frame.

5 Experiments

5.1 Experiment Setup

We conduct a wide range of experiments to test the phase transition ability of the proposed CPG model and the gait transition ability of the overall control framework. The physical and simulation robot model we used is shown in Fig. 7.

Table 1: Robot mechanical and simulation parameters

Mechanical Params.		**Simulation Contact Params.**	
Robot mass	2.218 kg	Stiffness	1×10^5 N/m
Body mass	0.88 kg	Force exponent	4.0
Leg mass	0.223 kg	Damping	1.0 Ns/m
Ipsilateral foot clearance	46 mm	Penetration Depth	0.01 m
Contralateral foot clearance	77 mm	Static Friction Coefficient	0.8
Body Length	134 mm	Kinetic Friction Coefficient	0.3

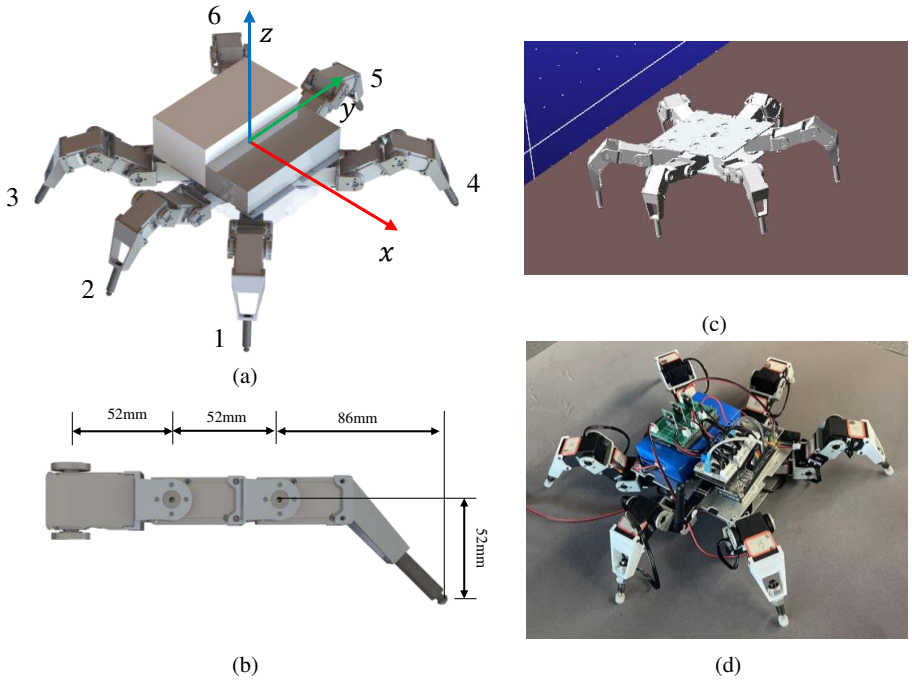

Fig. 7: An illustration of physical and simulation robot model. (a) The robot model with leg indexing and baselink coordinate drawing, (b) key dimensions the leg, (c) Adams virtual simulation model, (d) hexapod robot platform.

We use Adams to conduct the simulation experiments and gather key data for evaluation. Robot's mechanical parameters and its relevant simulation parameters are shown in Table 1.

Table 2: Robot hardware specifications

Hardware Component	**Version**	**Key Parameters**
Processing module	NVIDIA Jetson TX2	8GB 128-bit LPDDR4 Memory, Ubuntu 18.04 LTS, 7.5W / 15W
Carrier board	realtimes RSTO-9002U	USB type-C ports, 2× 3.3V UART +7V∼+19V voltage input
Battery	Hongfu Customized	12V, 5.2AH, 110mm×30mm×78mm
Bus servo	HINWONDER LX15D	6V∼8.4V, 17kg·cm, 43g
Buck Converter	Zaochen 7V5	4.5V∼27V voltage input, 7.5V voltage output, 3A working current

Table 3: Hexapod gaits, phase lags and duty cycles.

Gait	Desired Phase Lag θ_i (Neuron $1 \sim 6$)	Duty Cycle β
Tripod	π, π, π, π, π, π	0.5
Tetrapod	$2\pi/3$, $2\pi/3$, 0, $2\pi/3$, $2\pi/3$, $4\pi/3$	0.66
Wave	$2\pi/3$, $2\pi/3$, π, $2\pi/3$, $2\pi/3$, $\pi/3$	0.83
Caterpillar	$2\pi/3$, $2\pi/3$, $2\pi/3$, $2\pi/3$, $2\pi/3$, $2\pi/3$	0.6
Lurch	π, π, 0, π, π, 0	0.4
Metachronal	$\pi/3$, $\pi/3$, $\pi/3$, $\pi/3$, $\pi/3$, $\pi/3$	0.7

All software implementations are based on the Robot Operating System (ROS) running on an Ubuntu 18.04 environment, installed on an NVIDIA Jetson TX2 module. This module is paired with an RSTO-9002U carrier board, which utilizes three UART ports to communicate with the leg's BUS servo. The hardware specifications for the robot are detailed in Table 2.

For hexapod gait generation, we set $N = 6$ in Eq. (18). Moreover, we model the internal dynamics of each CPG neuron as Hopf oscillators with the dynamic equations:

$$\boldsymbol{F}(z_i) = \begin{bmatrix} O(x_i) \\ O(y_i) \end{bmatrix} = \begin{bmatrix} \alpha(\mu - x_i^2 - y_i^2)x_i - \omega_0 y_i \\ \beta(\mu - x_i^2 - y_i^2)y_i - \omega_0 x_i \end{bmatrix}, \tag{42}$$

where α,β controls the convergence speed to the limit cycle, ω_0, μ controls the angular frequency and the oscillation amplitude, respectively. According to proposition 2, we set $\gamma_i = N - i$ to prevent the phase-lock phenomenon during the transition process.

The desired phase lags and duty cycles of commonly observed gait patterns [11] in nature insects are list in Table 3.

In our gait transition experiments, we employ a Bézier curve-based method to ensure smooth adjustment of the parameter pair (β, θ_i) from the current gait specification to the target gait specification, thereby avoiding discontinuous or infeasible leg movements. As illustrated in Fig. 8, this curve is generated by four control points. Denoting a point on the curve as $B(p)$, where $p \in [0, 1]$ represents the progression of the curve, the gait specification parameters during the transition are defined as follows:

$$\beta(t) = \beta^- + (\beta^+ - \beta^-)B\left(\frac{t}{T_{ts}}\right), \quad \theta_i(t) = \theta_i^- + (\theta_i^+ - \theta_i^-)B\left(\frac{t}{T_{ts}}\right), \tag{43}$$

where T_{ts} denotes the duration of the gait transition. This formulation ensures a seamless transition, with both β and θ_i smoothly transitioning from their initial values (β^-, θ_i^-) to their final values (β^+, θ_i^+) over the transition period $[0, T_{ts}]$.

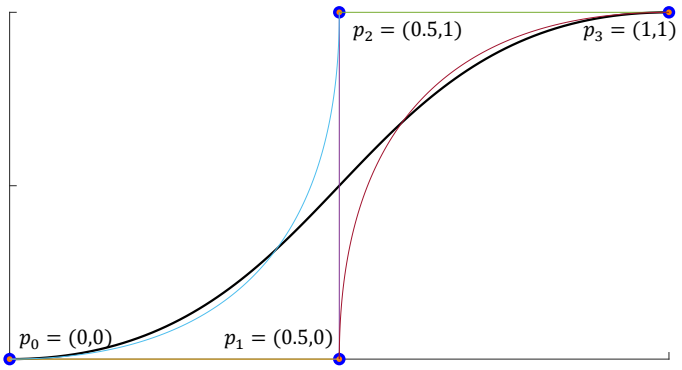

Fig. 8: An illustration showcasing the utilization of Bézier curves for the smooth adjustment of gait specification. The generated curve is depicted in black, while additional colored curves represent lower-order Bézier curves.

5.2 Phase Transition

The original diffusive CPG has been proven to transition quickly between tripod, tetrapod, and wave gaits. However, in this experiment, we demonstrate its limitation in transitioning between a wider range of gaits. Additionally, we showcase the ability of the proposed CPG framework to handle transitions across a broader range of gaits.

The results of gait transition tests on original diffusive-CPG are visualized in Fig. 9. It is apparent from Fig. 9a, 9b, and 9c that none of the transitions were successfully executed, as the phase relations of the oscillators remains unaltered (Fig. 9a and 9b) or wired (9c). These observed phenomena are consistent with the analysis presented in Section 2 as the transition from tripod to caterpillar and metachronal satisfies the Corollary 1.

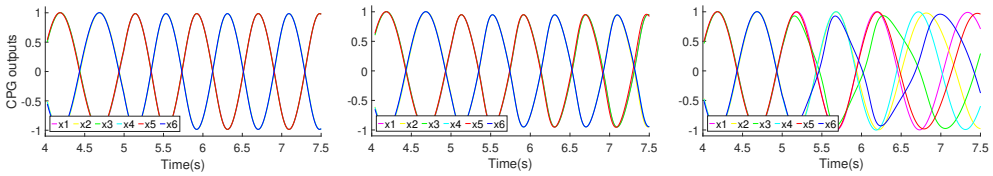

(a) (b) (c)

Fig. 9: Gait transition test of the original diffusive-CPG with structure parameters $\mu = 1$, $\alpha = 10$, $\beta = 10$, $\omega_0 = 2\pi$, and $\gamma = 2$. The phase lags are changed at $t = 5$s. x1-x6 are the outputs of the neurons in gait generator. (a) Transition test from tripod to caterpillar gait, (b) from tripod to metachronal gait, and (c) from tripod to lurch gait.

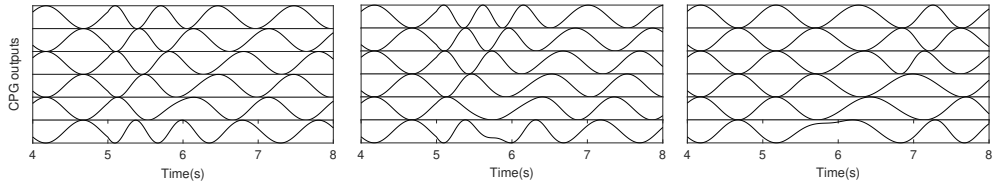

(a) (b) (c)

Fig. 10: Gait transition test of the proposed diffusive-CPG model with structure parameters $\mu = 1$, $\alpha = 10$, $\beta = 10$, $\omega_0 = 2\pi$ and $\gamma = 2$. The CPG outputs are $x_1 \sim x_6$ from the top to bottom. The phase lags are changed at $t = 5$s. (a) Transition from tripod to caterpillar gait, (b) transition from tripod to metachronal gait and (c) transition from tripod to lurch gait.

Fig. 10 presents the results of the gait transition test utilizing the proposed CPG. Evidently, our model effectively achieves gait transitions across all experimented scenarios. The transitions illustrate characteristics of both smoothness and speediness, as visible in every subplot. The desired phase can be subtly adjusted for practical implementation to fine-tune the transition dynamics even further.

5.3 Gait Transition

In this part, we undertake gait transition experiments for straight walking across various gait patterns, conducted both in simulation and on a physical robot. Our experiments involve comparing the efficacy of our proposed motion generation method with that of a vanilla approach. In the vanilla method, Bézier curves are solely employed for generating swing and stance trajectories, without accounting for stability criteria.

Throughout these experiments, we collect extensive data, including baselink's displacements, linear velocities and angular velocities. These metrics serve as indicators for evaluating the smoothness and stability of the gait transition process. By analyzing these data points, we can assess the effectiveness of our proposed method in ensuring

both smoothness and stability during gait transitions. The simulation results of transition from metachronal to tripod gait is shown in Fig. 11. In Fig. 11(a) and (b), it is evident that the robot, driven by the vanilla motion generation method, experiences significant tilting velocity fluctuations during the gait transition. Conversely, the proposed method demonstrates the ability to mitigate baselink tilting. The fluctuation during the transition profoundly impacts the robot's moving velocity, as observed in the grey plots (c). Comparing with the vanilla method, the proposed method effectively reduces velocity fluctuations, as depicted in the black plot (c). This reduction in velocity fluctuation diminishes foot slippage, consequently leading to a decrease in body displacement, as shown in the grey plot (d). With the proposed method, the resulting body displacement closely aligns with theoretical values, as illustrated by the black curves (d) in Fig. 11.

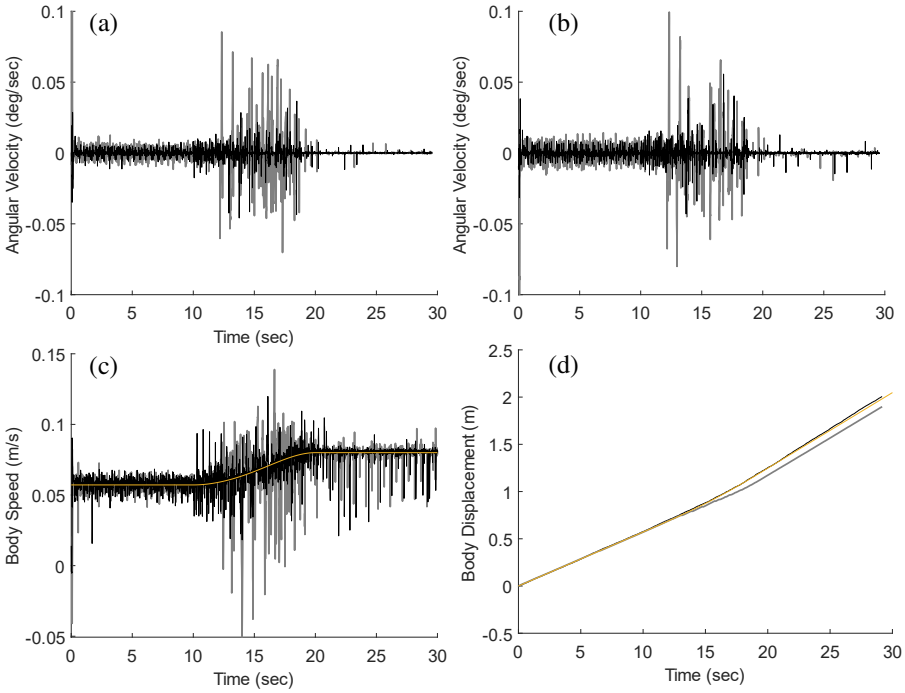

Fig. 11: The simulation results illustrating the transition from metachronal to tripod gait. The outcomes of the vanilla method, the proposed method, and the reference values are depicted in grey, black, and yellow, respectively. These results encompass the body's angular velocity around the baselink's x-coordinate, body's angular velocity around the baselink's y-coordinate (b), body speed (c) and body displacement (d).

With the enhanced phase transition capability of the proposed CPG model, we conduct the gait transition test for all other gait pairs. From the gathered data, we computed the deviations from the desired values to quantify the velocity fluctuations

relative to theoretical values. The results are presented in Table 4, where the numbers to the left of the "/" symbol correspond to the outcomes of the proposed method, while those to the right represent those of the vanilla method. Notably, with the exception of σ_{ω_x} during the transition between Wave and Lurch, the proposed gait transition method consistently yields significantly reduced velocity fluctuations compared to the vanilla motion generation approach.

Table 4: Variance Collection of different gait transition pairs.

Gait Pair	σ_{ω_x}	σ_{ω_y}	σ_v
Tripod-Wave	**0.0050**/0.0085	**0.0090**/0.0181	**0.0096**/0.0179
Tripod-Caterpillar	**0.0048**/0.0164	**0.0048**/0.0160	**0.0089**/0.0278
Tripod-Lurch	**0.0048**/0.0097	**0.0152**/0.0231	**0.0190**/0.0297
Tripod-Metachronal	**0.0065**/0.0150	**0.0058**/0.0159	**0.0092**/0.0218
Tripod-Tetrapod	**0.0033**/0.0114	**0.0044**/0.0155	**0.0033**/0.0114
Tetrapod-Wave	**0.0029**/0.0031	**0.0046**/0.0070	**0.0074**/0.0091
Tetrapod-Caterpillar	**0.0019**/0.0092	**0.0034**/0.0131	**0.0073**/0.0155
Tetrapod-Lurch	**0.0039**/0.0043	**0.0125**/0.0182	**0.0128**/0.0212
Tetrapod-Metachronal	**0.0039**/0.0085	**0.0051**/0.0089	**0.0082**/0.0114
Wave-Caterpillar	**0.0030**/0.0057	**0.0049**/0.0091	**0.0083**/0.0117
Wave-Lurch	0.0031/**0.0027**	**0.0139**/0.0171	**0.0152**/0.0210
Wave-Metachronal	**0.0034**/0.0077	**0.0045**/0.0072	**0.0079**/0.0104
Caterpillar-Lurch	**0.0013**/0.0033	**0.0139**/0.0244	**0.0193**/0.0287
Caterpillar-Metachronal	**0.0050**/0.0105	**0.0042**/0.0102	**0.0088**/0.0177
Lurch-Metachronal	**0.0039**/0.0062	**0.0136**/0.0177	**0.0145**/0.0227

For a clearer demonstration of our framework's gait transition capability, we present snapshots of the robot transitioning from tetrapod to caterpillar gait, along with the footprints and the z position of the right middle foot-tip in Fig. 12. As shown in Fig. 12a, the robot's gait patterns successfully transition from tetrapod to caterpillar. Additionally, during the gait transition, some legs exhibit narrower swing stages due to the automatic adjustment mechanism of the proposed framework, which enhances the robot's stability. The adjustment of the swing is more clearly illustrated in Fig. 12b. From the snapshots of the simulation and the physical experiments, we can clearly observe the progress of the gait transition (Fig. 12c). The snapshot at $t = 5$ seconds shows the robot's state before the transition. In the snapshots from $t = 10$ to $t = 20$ seconds, the relative positions of the contralateral feet gradually become in phase, indicating a successful transition to the caterpillar gait. Moreover, during the entire process, the robot's body shows almost no tilting, which further highlights the stability capability of the proposed framework.

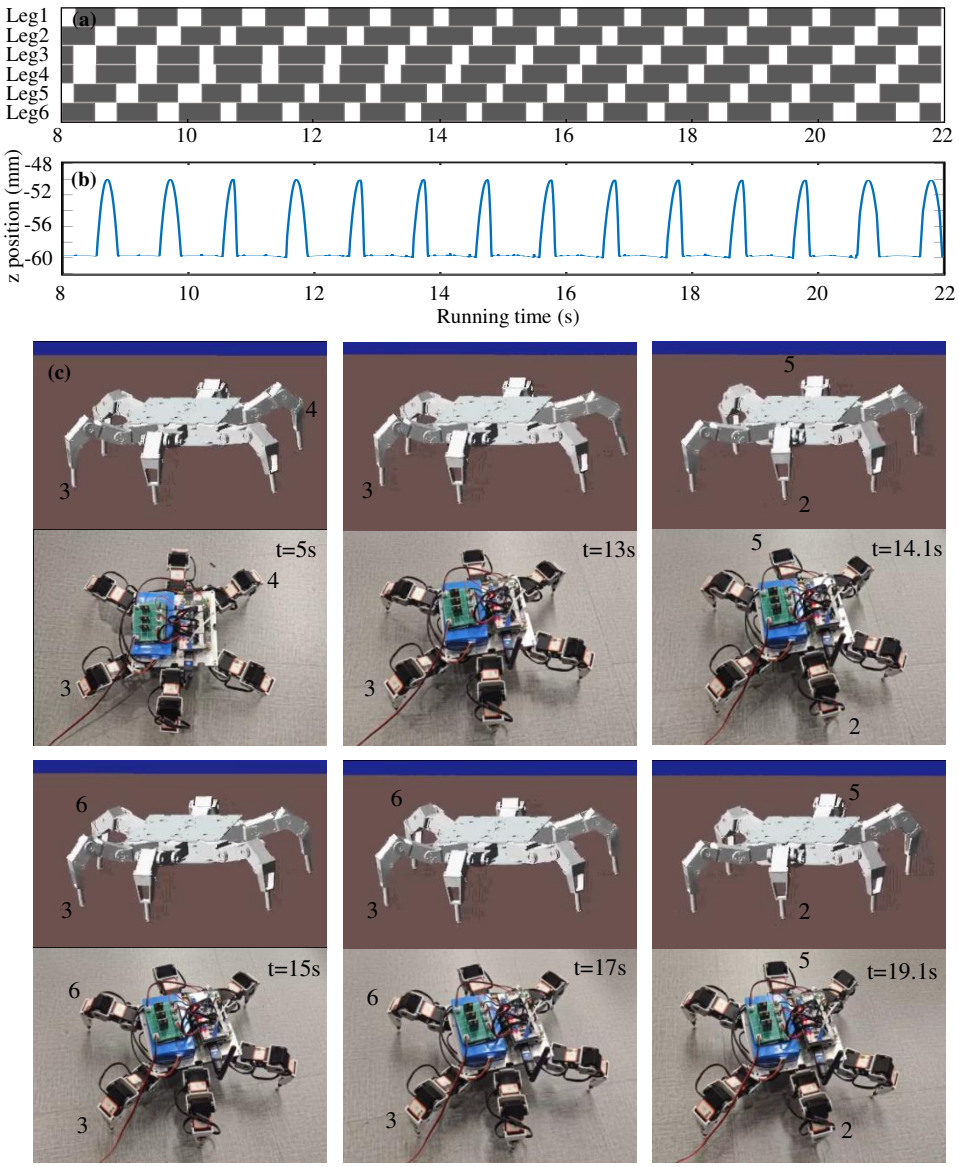

Fig. 12: Experimental results of the gait transition from tetrapod to caterpillar. (a) Resulting footprint diagram of the gait cycle. (b) The z position of the right middle foot w.r.t. baselink frame. (c) Snapshots during simulation and physical robot experiment.The gait transition starts at $t = 10s$ and end at $t = 20s$.

6 Conclusion

In conclusion, our study presents a novel and comprehensive control framework that addresses two core aspects of gait transition: phase transition and stable motion generation. The proposed CPG model enables fluid transitions across a wide range of gaits, endowing the robot with remarkable versatility in its locomotion. Simultaneously, our motion generator module ensures stable movement during these transitions. Experimental assessments in both simulation and real-world environments demonstrate that our method can execute transitions across various gaits with enhanced stability.

Future work will focus on incorporating more reasonable and feasible stability measures to drive the trajectory adjustment mechanism. Additionally, we aim to consider the robot's dynamics during transitions. For instance, when accelerating the swing process to gain more support, we must account for the generated inertia forces that may introduce instabilities. More refined motion generation methods, or even learning-based approaches that consider these aspects, need to be explored.

Supplementary information. The experimental videos and data are uploaded in the supplementary material.

Declarations

This research was supported by the Intelligent Aerospace System Leading Innovation Team Program of Zhejiang (Grant No. 2022R01003)

References

[1] Anderson, Shultz, Jayne: Axial kinematics and muscle activity during terrestrial locomotion of the centipede scolopendra heros. The Journal of Experimental Biology **198 Pt 5** (1995)

[2] Jamon, Clarac: Locomotor patterns in freely moving crayfish (procambarus clarkii). The Journal of Experimental Biology **198 Pt 3**, 683–700 (1995)

[3] Weihmann, T., Brun, P.-G., Pycroft, E.: Speed dependent phase shifts and gait changes in cockroaches running on substrates of different slipperiness. Frontiers in Zoology **14** (2017)

[4] Zhao, J., Zhu, F., Yan, S.: Honeybees prefer to steer on a smooth wall with tetrapod gaits. Journal of Insect Science **18** (2018)

[5] Grillner, S.: Locomotion in vertebrates: central mechanisms and reflex interaction. Physiological Reviews **55 2**, 247–304 (1975)

[6] Herman, R.M., Grillner, S., Stein, P.S.G., Stuart, D.G.: Neural control of locomotion. In: Advances in Behavioral Biology (1976)

[7] Golubitsky, M., Stewart, I., Schaeffer, D.G.: Singularities and Groups in Bifurcation Theory: Volume II. Springer, New York (2012)

[8] Song, Z., Huang, X., Xu, J.: Spatiotemporal pattern of periodic rhythms in delayed van der pol oscillators for the CPG-based locomotion of snake-like robot. Nonlinear Dynamics **110**, 3377–3393 (2022)

[9] Buono, P.-L., Golubitsky, M.: Models of central pattern generators for quadruped locomotion i. primary gaits. Journal of Mathematical Biology **42**, 291–326 (2001)

[10] Righetti, L., Ijspeert, A.J.: Pattern generators with sensory feedback for the control of quadruped locomotion. 2008 IEEE International Conference on Robotics and Automation, 819–824 (2008)

[11] Pinto, C.M., Rocha, D., Santos, C.P.: Hexapod robots: new CPG model for generation of trajectories. J. Numer. Anal. Ind. Appl. Math **7**(24), 15–26 (2012)

[12] Sartoretti, G., Shaw, S., Lam, K., Fan, N., Travers, M., Choset, H.: Central pattern generator with inertial feedback for stable locomotion and climbing in unstructured terrain. In: 2018 IEEE International Conference on Robotics and Automation (ICRA), pp. 5769–5775 (2018)

[13] Xiao, W., Wang, W.: Hopf oscillator-based gait transition for a quadruped robot. 2014 IEEE International Conference on Robotics and Biomimetics (ROBIO 2014), 2074–2079 (2014)

[14] Yu, H., Gao, H., Ding, L., Li, M., Deng, Z., Liu, G.: Gait generation with smooth transition using CPG-based locomotion control for hexapod walking robot. IEEE Transactions on Industrial Electronics **63**, 5488–5500 (2016)

[15] Darbha, N.H.: An optimization strategy for hexapod gait transition. Master's thesis, Wright State University (2017)

[16] Bai, L., Hu, H., Chen, X., Sun, Y., Ma, C., Zhong, Y.: CPG-based gait generation of the curved-leg hexapod robot with smooth gait transition. Sensors **19**(17), 3705 (2019)

[17] Shaw, S., Sartoretti, G.: Keyframe-based CPG for stable gait design and online transitions in legged robots. In: 2022 IEEE 61st Conference on Decision and Control (CDC), pp. 756–763 (2022). IEEE

[18] Farin, G., Hansford, D.: The Essentials of CAGD. AK Peters/CRC Press, Boca Raton, London, New York (2000)

[19] Papadopoulos, E., Rey, D.A.: A new measure of tipover stability margin for mobile manipulators. Proceedings of IEEE International Conference on Robotics and Automation **4**, 3111–3116 (1996)

[20] Nakanishi, J., Cory, R.E., Mistry, M.N., Peters, J., Schaal, S.: Operational space control: A theoretical and empirical comparison. The International Journal of Robotics Research **27**, 737–757 (2008)

Supplementary Files

This is a list of supplementary files associated with this preprint. Click to download.

- experimentvideos.zip
- matlab.zip